



## Structural Biology

## From Peptide Fragments to Whole Protein: Copper(II) Load and Coordination Features of IAPP

Antonio Magri,<sup>\*,[a]</sup> Adriana Pietropaolo,<sup>[b]</sup> Giovanni Tabbi,<sup>[a]</sup> Diego La Mendola,<sup>\*,[c]</sup> and Enrico Rizzarelli<sup>[a, d]</sup>

**Abstract:** The copper-binding features of rat islet amyloid polypeptide (r-IAPP) are herein disclosed through the determination of the stability constants and spectroscopic properties of its copper complex species. To mimic the metal binding sites of the human IAPP (h-IAPP), a soluble, single-point mutated variant of r-IAPP, having a histidine residue in place of Arg18, was synthesized, that is, r-IAPP(1–37; R18H). The peptide IAPP(1–8) was also characterized to have deeper insight into the N-terminus copper(II)-binding features of r-IAPP as well as of its mutated form. A combined experimental (thermodynamic and spectroscopic) and computational approach allowed us to assess the metal loading and the coordination features of the whole IAPP. At physiological pH, the N-terminal amino group is the Cu<sup>2+</sup> main binding site both of entire r-IAPP and of its mutated form that mimics h-IAPP. The histidine residue present in this mutated polypeptide accounts for the second Cu<sup>2+</sup> binding. We can speculate that the copper driven toxicity of h-IAPP in comparison to that of r-IAPP can be attributed to the different metal loading and the presence of a second metal anchoring site, the His<sub>18</sub>, whose role is usually invoked in the process of h-IAPP aggregation.

Amylin or human islet amyloid polypeptide (h-IAPP) is a 37 residues (Scheme S1 in the Supporting Information) hormone peptide. It is stored inside the pancreatic  $\beta$ -cell granules<sup>[1]</sup> and

released with insulin in response to elevated blood glucose levels.<sup>[2–4]</sup>

h-IAPP is an intrinsically disordered protein in solution as a monomer, but forms toxic oligomers, fibrils, and extracellular amyloid deposits in the  $\beta$ -cells—found in most type 2 diabetes patients.<sup>[5,6]</sup> Recently, the interest was focused on the aggregation of small IAPP oligomers and not on the mature fibrils.<sup>[7–9]</sup> Increasing amounts of experimental and theoretical results suggests that the toxic species of IAPP are present exclusively as small oligomers, which are also responsible for disruption of membrane permeability and metal ion homeostasis impairment.<sup>[8–10]</sup> The sequence 20–29 is considered the most amyloidogenic and together with regions 30–37 and 8–20 can contribute to the formation of amyloid fibrils.<sup>[11]</sup> On the other hand, the intact disulfide bond present in the 1–8 domain may be protective against aggregation due to a decrease of inter-peptide hydrogen bonding.<sup>[12]</sup>

Differently from human, the rat amylin r-IAPP has a reduced amyloidogenic tendency, showing a peculiar analogy with the behavior of rat  $\beta$ -amyloid in comparison with human A $\beta$ .<sup>[13]</sup> This may be due to the presence both of three Pro residues<sup>[14]</sup> and the substitution of His<sub>18</sub> by an Arg in the primary sequence. Although His<sub>18</sub> does not belong to the amyloidogenic region, it plays a key role during the process of h-IAPP aggregation in particular i) modulating the orientation of the polypeptide IAPP in the membrane<sup>[15–18]</sup> and ii) interacting with Zn<sup>2+</sup> and Cu<sup>2+</sup>.<sup>[19–29]</sup>

Zinc-IAPP complex formation i) promotes the IAPP oligomer formation; ii) at the same time, creates a barrier for the formation of amyloid fibrils. It is interesting to note that Zn<sup>2+</sup> showed an ambiguous behavior on IAPP fibrils formation. At high metal concentration, the lag-time of fibrils formation changed with an acceleration of the addition of IAPP to pre-formed fibrils whereas the opposite situation is observed at Zn<sup>2+</sup> low concentrations.<sup>[30]</sup>

Copper metabolism is associated with the pathological mechanism of amyloidosis in diabetes,<sup>[31]</sup> but the Cu<sup>2+</sup> impact on human amylin is characterized by conflicting findings, related with increased and decreased copper-mediated h-IAPP cytotoxicity.<sup>[23, 24, 27, 32–34]</sup>

The promotion or inhibition of h-IAPP aggregation by Cu<sup>2+</sup> binding has recently been proposed to depend by metal ion concentration,<sup>[7]</sup> suggesting that different metal complex species can be responsible of contrasting results. The coordination features of Cu<sup>I</sup> complexes with different human amylin peptide fragments have thus been investigated, focusing mainly

[a] Dr. A. Magri, Dr. G. Tabbi, Prof. E. Rizzarelli  
Istituto di Biostrutture e Bioimmagini-CNR  
Via P. Gaifami 18, 95126 Catania (Italy)  
E-mail: leotony@unicat.it

[b] Dr. A. Pietropaolo  
Dipartimento di Scienze della Salute  
Università "Magna Graecia" di Catanzaro  
Campus Universitario, Viale Europa, 88100 Catanzaro (Italy)

[c] Prof. D. La Mendola  
Dipartimento di Farmacia, Università di Pisa  
Via Bonanno Pisano 6, 56126 Pisa (Italy)  
E-mail: diego.lamendola@unipi.it

[d] Prof. E. Rizzarelli  
Dipartimento di Scienze Chimiche, Università di Catania  
Viale A. Doria, 5, 95125 Catania (Italy)

Supporting information and the ORCID identification number(s) for the author(s) of this article can be found under <https://doi.org/10.1002/chem.201704910>.

on the amyloidogenic central region of the polypeptide.<sup>[35]</sup> There is not, however, general agreement on the metal loading and the amino acid residues, involved in copper binding.<sup>[22,28,29]</sup> In an attempt to overcome the contrasting findings, the focus was shifted from peptide fragments to whole IAPP. Here we report on the Cu<sup>II</sup> binding properties of r-IAPP(1–37) (L) and a modified r-IAPP(1–37) named r-IAPP(1–37;R18H) (L') in which the Arg<sub>18</sub> residue was replaced by an His, to mimic all the h-IAPP metal binding sites and to overcome its solubility limits. The Cu<sup>II</sup> complexes formed with the octapeptide encompassing the first eight amino acid residues (K-c.[CNTATC]A-NH<sub>2</sub>) of IAPPs (L'') was also characterized by an experimental and computational approach to give more details on the metal coordination environment.

Combined potentiometric titrations and spectroscopic techniques—circular dichroism (CD), UV/Vis, and EPR—were employed to obtain speciation, affinity, and binding features of the copper(II) complexes with the three IAPP peptides at different molar ratios (Cu/IAPP 1:1 and 2:1).

Both L and L' are soluble at millimolar concentration up to pH 8.5, above which precipitation occurred. For this reason, the determination of the pK values of the most basic protonation sites failed (Table S1). The distribution diagrams (Figure 1) of the Cu<sup>II</sup>-L and Cu<sup>II</sup>-L'' systems in a clear manner show that both polypeptides give rise to the same set of metal complex species with similar stability constants (Table S2).

In L and L'', the amine nitrogen of the N-terminal domain is the only anchoring site for Cu<sup>2+</sup>. The [CuL] affinity constant value (log β = 4.92) is consistent with a N,O(NH<sub>2</sub>, CO)-metal coordination mode, with the involvement of the amine nitrogen and the Asn3 carbonyl group, in keeping with what found in similar systems.<sup>[36]</sup> The octapeptide fragment shows a stability constant value (log β = 4.97) similar to that found for the entire polypeptide, suggesting the same metal binding environment.

The Cys<sub>2</sub>-Cys<sub>7</sub> intramolecular bridge assists the subsequent complex species [CuLH<sub>2</sub>] and [CuL''H<sub>2</sub>] formation, characterized by a Cu<sup>2+</sup>-driven dual cooperative amide deprotonation, as also found for other disulfide bridge containing peptide systems.<sup>[37]</sup>

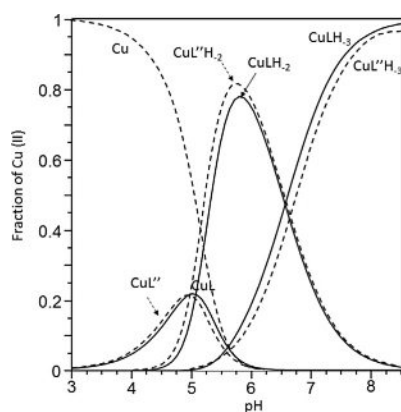


**Figure 1.** Distribution diagrams for Cu<sup>2+</sup>-L (solid line) and Cu<sup>2+</sup>-L'' (dashed line) systems, respectively. ([Cu<sup>2+</sup>] = [L] = [L''] = 1 mM).

Disulfide bridge also favored the deprotonation of the third peptide nitrogen atom (see DFT calculations) with the formation of [CuLH<sub>3</sub>] and [CuL''H<sub>3</sub>], which are the main species at physiological pH.

The nearly perfect overlap of deconvoluted CD and UV/Vis spectra of complex species pairs [CuLH<sub>2</sub>], [CuL''H<sub>2</sub>] (Figure 2) and [CuLH<sub>3</sub>], [CuL''H<sub>3</sub>] (Figure 3) highlight that similar donor atom sets were involved in the Cu<sup>2+</sup> coordination.

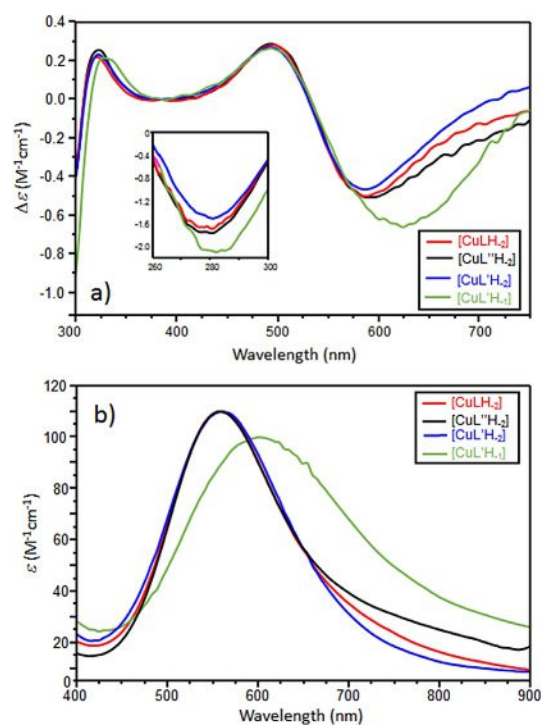


**Figure 2.** Deconvoluted CD (a) and UV/Vis (b) spectra of the main Cu<sup>2+</sup> complex species formed in the 4.8–6 pH range. Inset shows CT bands (260–300 nm).

CD, UV, and potentiometric data are indicative of a 3 N {NH<sub>2</sub>, 2 N<sup>-</sup>} coordination mode<sup>[37]</sup> adopted by [CuLH<sub>2</sub>] and [CuL''H<sub>2</sub>]. Further support comes from the low g<sub>||</sub> and the high parallel hyperfine coupling constant values (g<sub>||</sub> = 2.198, A<sub>||</sub> = 201 × 10<sup>-4</sup> cm<sup>-1</sup> for [CuLH<sub>2</sub>] and g<sub>||</sub> = 2.204, A<sub>||</sub> = 204 × 10<sup>-4</sup> cm<sup>-1</sup> for [CuL''H<sub>2</sub>]). In these species, Cu<sup>2+</sup> binds to terminal NH<sub>2</sub> and to two amide deprotonated nitrogen atoms in a nearly planar arrangement. The fourth equatorial position is likely completed by a peptide carbonyl group.<sup>[37]</sup>

The Hamiltonian parameters of EPR spectra of [CuLH<sub>3</sub>] and [CuL''H<sub>3</sub>] species show a further decrease of the g<sub>||</sub> values accompanied with a slight increase of the A<sub>||</sub> values (Table S3). These parameters are consistent with the involvement of four nitrogen atoms in a {NH<sub>2</sub>, 3 N<sup>-</sup>} coordination mode. Cu<sup>2+</sup> experiences slightly distorted planar environment as also confirmed by the increase of the ε value and the shift of λ<sub>max</sub>.<sup>[36,37]</sup> Potentiometric and spectroscopic results indicate without doubt that L'' is a representative model of the entire r-IAPP copper binding features. DFT calculations were carried on Cu<sup>II</sup>-L'' system in order to determine the coordination geometry in

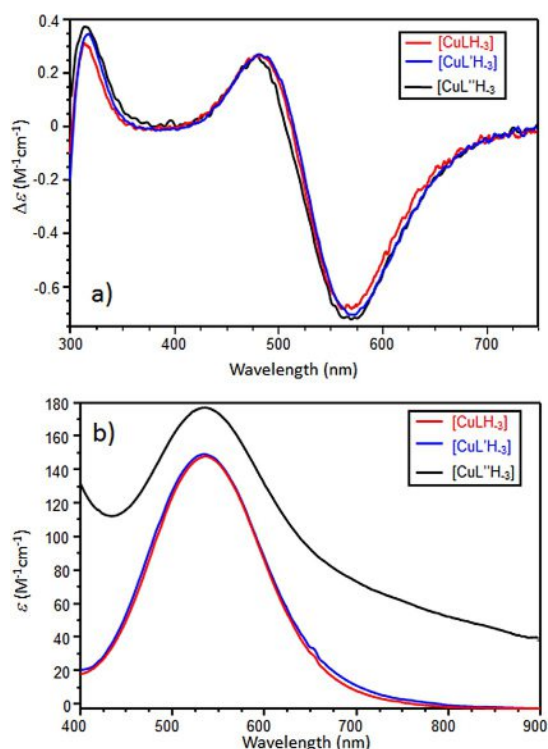


**Figure 3.** Deconvoluted CD (a) and UV/Vis (b) spectra of the main  $\text{Cu}^{2+}$  complex species formed with the three polypeptides at physiological pH; the value of  $\epsilon_{\text{max}}$  for  $[\text{CuL}''\text{H}_3]$  was altered by the presence of a precipitate.

the N-terminus and the specific amide nitrogen atoms involved in the  $[\text{CuL}''\text{H}_2]$  and  $[\text{CuL}''\text{H}_3]$  species.

The  $\text{L}''$  conformations sampled from Parallel Tempering simulations show  $\beta$ -turn domains within the  ${}^4\text{TATC}^7$  sequence. The peptide secondary structure is rigid with essentially one main cluster with 98% of population (Figure 4a) and a second low adopted cluster with 2% of population (Figure 4b). The rigidity arises from the presence of a disulfide bridge involving  $\text{Cys}_2$  and  $\text{Cys}_7$ . Upon  $\text{Cu}^{2+}$  coordinates within  $\text{L}''$ , the beta turn domains are still adopted, allowing the formation of a coordination polyhedron within the peptide cycle formed by the disulfide bridge in which the  $\text{Cu}^{2+}$  ion can coordinate up to three amide groups. In particular, the  $[\text{CuL}''\text{H}_2]$  species involves the N-terminal group, the second and the third amide groups belonging, respectively to  $\text{Cys}_2$  and  $\text{Asn}_3$  and an inner-shell water molecule (Figure 4c). The water molecule is then replaced by a fourth amide group belonging to  $\text{Thr}_4$  (Figure 4d). Herein, the coordination polyhedron is more distorted because the insertion of the amide belonging to  $\text{Thr}_4$  causing an increasing in the bending angle of 9.68 degrees (109.43 in the  $[\text{CuL}''\text{H}_3]$  vs. 99.75 in the  $[\text{CuL}''\text{H}_2]$  species, Table S4).

In Figure 5a, the distribution diagram for the  $\text{Cu}^{\text{II}} \text{Cu}^{2+}\text{-L}'$  system at  $\text{ML}^{-1}$  ratio 1:1 until pH 8.5 is reported. Above this pH value, precipitation was observed. The stability constants and the spectroscopic parameters for these complex species are reported in Tables S2 and S3 in the Supporting Information, respectively.

Significant differences were found for  $\text{Cu}^{2+}\text{-L}'$  system respect to  $\text{Cu}^{2+}\text{-L}$  and  $\text{Cu}^{2+}\text{-L}''$  systems, as expected due to

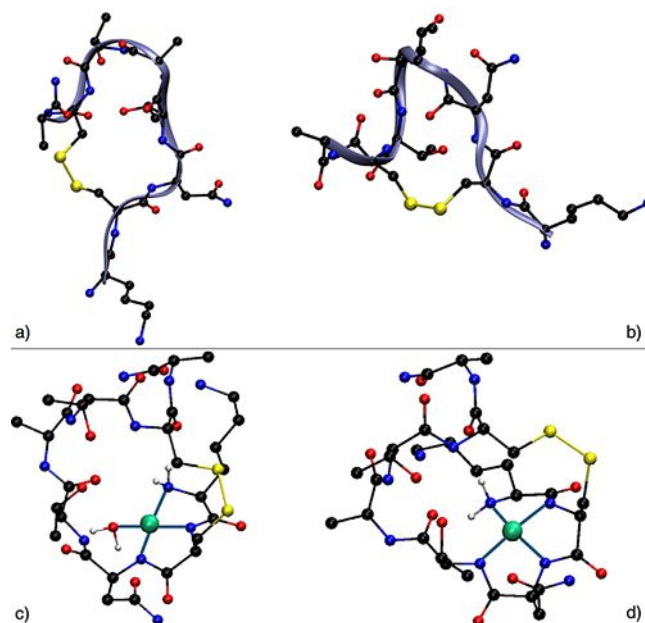


**Figure 4.** The two most adopted conformations of  $\text{L}''$  sampled from parallel tempering simulations, respectively with 98% (a) and 2% (b) of population. The coordination polyhedra of  $\text{Cu}^{2+}$  within the  $\text{L}''$  peptide, respectively with two c) and three d) deprotonated amides.  $\text{Cu}^{2+}$  is shown in green, N in blue, S in yellow, C in black and O in red.

the presence of a second metal binding site represented by  $\text{His}_{18}$ .

$[\text{CuL}']$  is the first detected species; its  $\log \beta$  value (6.19) suggests a 2 N metal coordination mode. Both the terminal  $\text{NH}_2$  and the imidazole ring nitrogen are involved in metal binding, forming a macrochelate ring, as found for other similar polypeptides.<sup>[36]</sup>

Increasing the pH,  $[\text{CuL}'\text{H}_1]$  is formed and it is characterized by a 3 N coordination mode  $\{\text{NH}_2, \text{N}_{\text{im}}, \text{N}^-\}$ . The second binding site favors the deprotonation of a single amide nitrogen, differently from the other two peptides, which form a species with two deprotonated amide nitrogen atoms in the same pH range. The deconvoluted d-d band is centred at 605 nm (Figure 2b, green trace) as observed for other  $\text{Cu}^{2+}$  linear peptide systems adopting this coordination mode.<sup>[38,39]</sup>

Deconvoluted CD spectrum (Figure 2a, green trace) showed a negative d-d band centred at 625 nm and a charge transfer negative band centred at 282 nm, diagnostic of the involvement of  $\text{NH}_2$  in the copper(II) coordination.

Clues about the coordination of  $\text{His}_{18}$  by its imidazole nitrogen can be found in the positive band centered at 330 nm, which includes the contribution of the  $\text{N}_{\text{im}} \rightarrow \text{Cu}^{2+}$  charge-transfer (CT) band that is red-shifted with respect to the dichroic band centered at 320 nm, ascribed to the  $\text{N}_{\text{amide}} \rightarrow \text{Cu}^{2+}$  CT band in the  $\text{L}$  and  $\text{L}''$  systems.

Further support on the involvement of imidazole nitrogen in copper(II) ion binding comes from  $[\text{CuL}'\text{H}_1]$  EPR parameters ( $g_{\parallel} = 2.222$ ,  $A_{\parallel} = 153 \times 10^{-4} \text{ cm}^{-1}$ ). These values are indicative of the involvement of three nitrogen atoms and are related with either a square-pyramidal or a tetrahedral distorted square-planar coordination geometry.<sup>[40]</sup> Furthermore, these EPR pa-

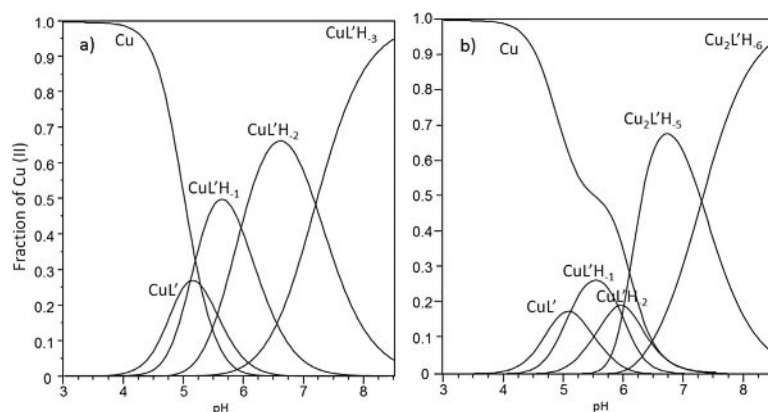
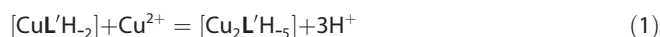


Figure 5. Distribution diagrams for  $\text{Cu}^{2+}$ - $\text{L}'$  system at metal to ligand ratios of a) 1:1 and b) 2:1.

rameters are very similar to those reported for the analogous species having a  $\{\text{NH}_2, \text{N}^-, \text{N}_{\text{im}}, \text{CO}\}$  metal coordination mode.<sup>[38]</sup>

Increasing the pH, the formation of  $[\text{CuL}'\text{H}_2]$  followed by  $[\text{CuL}'\text{H}_3]$  was found. These two species reached their maximum formation percentage at pH 6.5 and 8.5, respectively. The pK values of these two species (Table S2) are consistent with two consecutive amide nitrogen deprotonation steps forming 3 N  $\{\text{NH}_2, 2 \text{N}^-\}$  and 4 N  $\{\text{NH}_2, 3 \text{N}^-\}$  metal coordination environments, respectively, assisted by the concomitant  $\text{Cu}^{2+}$  imidazole nitrogen bond breaking. CD, UV/Vis, and EPR parameters determined for  $[\text{CuL}'\text{H}_2]$  and  $[\text{CuL}'\text{H}_3]$  support the above-indicated coordination modes (Table S1). Their CD and UV/Vis spectra are superimposable with those obtained for the corresponding metal complex species formed by  $\text{L}$  and  $\text{L}''$ , respectively (Figures 2 and 3). EPR parameters suggest the formation of two chelate rings involving  $\text{NH}_2$  and two or three deprotonated amide nitrogen atoms. Thus the three peptides are characterized by the same metal binding sites without the involvement of  $\text{His}_{18}$  at 1:1 metal to ligand ratio, also by  $\text{L}'$ , the single mutated r-IAPP.

Increasing the metal to ligand ratio,  $\text{L}'$  was able to coordinate two  $\text{Cu}^{2+}$  ions. Until pH 5.5–6, aside from free  $\text{Cu}^{\text{II}}$  ion (60%), three mono complex species were present, that is,  $[\text{CuL}']$ ,  $[\text{CuL}'\text{H}_1]$  and  $[\text{CuL}'\text{H}_2]$ , whereas the first binuclear  $[\text{Cu}_2\text{L}'\text{H}_5]$  species formed above pH 6 (Figure 5b). This species became the predominant species and reached its maximum formation percentage at pH 6.75. The coordination of a second metal ion involves the deprotonation of three additional amide nitrogen atoms with respect to the two present in the  $[\text{CuL}'\text{H}_2]$  complex species, according to the stepwise equilibrium [Equation (1)]:



The  $\log K$  value calculated according to this step equilibrium ( $\log K = \log \beta[\text{Cu}_2\text{L}'\text{H}_5] - \log \beta[\text{CuL}'\text{H}_2] = -15.11$ ) results in a significantly different value from the affinity constant value of  $[\text{CuL}'\text{H}_3]$  (Table S2). In contrast, this value agrees with those previously found for the analogous deprotonated species formed by  $\text{Cu}^{2+}$  ion with Ac-PEG-h-IAPP(14–22)- $\text{NH}_2$  ( $\log \beta =$

$-15.80$ ).<sup>[26]</sup> The binding of the second  $\text{Cu}^{2+}$  is anchored to the  $\text{His}_{18}$  residue that drives the deprotonation processes towards the N-terminus. Though we are aware that isomeric species can contribute to the  $[\text{Cu}_2\text{L}'\text{H}_5]$  binding features, the spectroscopic results support the cooperative deprotonation process centered on  $\text{His}_{18}$  with the second  $\text{Cu}^{\text{II}}$  ion that experiences a  $(\text{N}_{\text{im}}, 3 \text{N}^-)$  binding mode, whereas the first copper(II) ion shows a  $(\text{NH}_2, 2 \text{N}^-)$  coordination environment. UV/Vis parameters determined for  $[\text{Cu}_2\text{L}'\text{H}_5]$  (Table S5) evidenced a red shift of the d–d band (Figure S1).

Increasing the pH, a deprotonation of another amide nitrogen atom occurred and the  $[\text{Cu}_2\text{L}'\text{H}_6]$  formed and reached its maximum formation percentage at pH 8.  $[\text{Cu}_2\text{L}'\text{H}_5]$  and  $[\text{Cu}_2\text{L}'\text{H}_6]$  are the two complex species present at physiological pH. The  $\log K$  value of this deprotonation process ( $\log K = \log \beta[\text{Cu}_2\text{L}'\text{H}_6] - \log \beta[\text{Cu}_2\text{L}'\text{H}_5] = -11.36$ ) is similar to that found for the formation of  $[\text{CuL}'\text{H}_3]$  (Table S2), indicating that a  $\{\text{NH}_2, 3 \text{N}^-\} + \{\text{N}_{\text{im}}, 3 \text{N}^-\}$  coordination mode is adopted by the metal ion in  $[\text{Cu}_2\text{L}'\text{H}_6]$  as corroborated by UV/Vis and CD data (Table S3).

In summary, the study of the copper(II) ion binding with the whole r-IAPP and its mutant that can mimic all the metal anchoring sites of h-IAPP, allowed us to assess both  $\text{Cu}^{2+}$  loading and coordination features of these IAPP variants. It is possible to speculate that the dependence of IAPP toxicity by the metal to polypeptide molar ratio can be rationalized on the basis of these results, being also aware that new experiments should be designed to support this hypothesis. Indeed, potentiometric measurements on the whole IAPP complex with zinc ions are currently in progress so to compare with data here reported.

## Acknowledgements

Authors thank the University Consortium for Research in the Chemistry of Metal ions in Biological Systems (CIRCMSB).

## Conflict of interest

The authors declare no conflict of interest.

**Keywords:** copper · DFT · diabetes · IAPP · potentiometry

- [1] A. Lukinius, E. Wilander, G. T. Westermark, U. Engstrom, P. Westermark, *Diabetologia* **1989**, *32*, 240–244.
- [2] A. Young, *Adv. Pharmacol.* **2005**, *52*, 19–45.
- [3] P. Moreno, A. Acitores, I. Gutiérrez-Rojas, B. Nuche-Berenguer, M. El As-sar, L. Rodríguez-Manas, R. Gomis, I. Valverde, M. Visa, W. J. Malaisse, A. Novials, N. González, M. L. Villanueva-Peñacarrillo, *Peptides* **2011**, *32*, 2077–2085.
- [4] W. A. Banks, A. J. Kastin, L. M. Maness, W. Huang, J. B. Jaspan, *Life Sci.* **1995**, *57*, 1993–2001.
- [5] B. Konarkowska, J. F. Aitken, J. Kistler, S. P. Zhang, G. J. S. Cooper, *FEBS J.* **2006**, *273*, 3614–3624.
- [6] P. Westermark, A. Andersson, G. T. Westermark, *Physiol. Rev.* **2011**, *91*, 795–826.
- [7] P. Nedumpully-Govindan, Y. Yang, R. Andorfer, W. Cao, F. Ding, *Biochemistry* **2015**, *54*, 7335–7344.
- [8] J. R. Brender, S. Salamekh, A. Ramamoorthy, *Acc. Chem. Res.* **2012**, *45*, 454–462.
- [9] H. Patel, A. S. Pithadia, J. R. Brender, C. A. Fierke, A. Ramamoorthy, *J. Phys. Chem. Lett.* **2014**, *5*, 1864–1870.
- [10] G. Pappalardo, D. Milardi, A. Magri, F. Attanasio, G. Impellizzeri, C. La Rosa, D. Grasso, E. Rizzarelli, *Chem. Eur. J.* **2007**, *13*, 10204–10215.
- [11] E. Jaikaran, A. Clark, *Biochim. Biophys. Acta Mol. Basis Dis.* **2001**, *1537*, 179–203.
- [12] A. I. Ilitchev, M. J. Giammona, T. O. Do, A. G. Wong, S. K. Buratto, J. E. Shea, D. P. Raleigh, M. T. Bowers, *J. Am. Soc. Mass Spectrom.* **2016**, *27*, 1010–1018.
- [13] A. N. Istrate, P. O. Tsvetkov, A. B. Mantsyzov, A. A. Kulikova, S. A. Kozin, A. A. Makarov, V. I. Polshakov, *Biophys. J.* **2012**, *102*, 136–143.
- [14] P. Westermark, U. Engstroem, K. H. Johnson, G. T. Westermark, C. Betsholtz, *Proc. Natl. Acad. Sci. USA* **1990**, *87*, 5036–5040.
- [15] A. Abedini, D. P. Raleigh, *Biochemistry* **2005**, *44*, 16284–16291.
- [16] Y. Li, W. Xu, Y. Mu, J. Z. Zhang, *J. Chem. Phys.* **2013**, *139*, 055102.
- [17] J. R. Brender, K. Hartman, K. R. Reid, R. T. Kennedy, A. Ramamoorthy, *Biochemistry* **2008**, *47*, 12680–12688.
- [18] R. P. R. Nanga, J. R. Brender, J. Xu, G. Veglia, A. Ramamoorthy, *Biochemistry* **2008**, *47*, 12689–12697.
- [19] L. Rivillas-Acevedo, C. Sánchez-López, C. Amero, L. Quintanar, *Inorg. Chem.* **2015**, *54*, 3788–3796.
- [20] A. Sinopoli, A. Magri, D. Milardi, M. Pappalardo, P. Pucci, A. Flagiello, J. J. Titman, V. G. Nicoletti, G. Caruso, G. Pappalardo, G. Grasso, *Metallomics* **2014**, *6*, 1841–1852.
- [21] J. R. Brender, J. Krishnamoorthy, G. F. M. Messina, A. Deb, J. E. Penner-Hahn, S. Vivekanandan, C. La Rosa, A. Ramamoorthy, *Chem. Commun.* **2013**, *49*, 3339–3341.
- [22] J. R. Brender, K. Hartman, R. P. Nanga, N. Popovych, R. de La Salud Bea, S. Vivekanandan, E. N. Marsh, A. Ramamoorthy, *J. Am. Chem. Soc.* **2010**, *132*, 8973–8983.
- [23] B. Ward, K. Walker, C. Exley, *J. Inorg. Biochem.* **2008**, *102*, 371–375.
- [24] L. Ma, X. Li, Y. Wang, W. Zheng, T. Chen, *J. Inorg. Biochem.* **2014**, *140*, 143–152.
- [25] M.-J. Kim, H.-T. Kim, *Eur. J. Mass Spectrom.* **2012**, *18*, 51–58.
- [26] A. Masad, B. J. Tabner, J. Mayes, D. Allsop, *Free Radical Biol. Med.* **2011**, *51*, 869–875.
- [27] Y. P. Yu, P. Lei, J. Hu, W. H. Wu, Y. F. Zhao, Y. M. Li, *Chem. Commun.* **2010**, *46*, 6909–6911.
- [28] A. Magri, D. La Mendola, V. G. Nicoletti, G. Pappalardo, E. Rizzarelli, *Chem. Eur. J.* **2016**, *22*, 13287–13300.
- [29] C. Sánchez-López, R. Cortés-Mejía, M. C. Miotto, A. Binolfi, C. O. Fernández, J. M. del Campo, L. Quintanar, *Inorg. Chem.* **2016**, *55*, 10727–10740.
- [30] S. Salamekh, J. R. Brender, S.-J. Hyung, R. P. R. Nanga, S. Vivekanandan, B. T. Ruotolo, A. Ramamoorthy, *J. Mol. Biol.* **2011**, *410*, 294–306.
- [31] A. Tanaka, H. Kaneto, T. Miyatsuka, K. Yamamoto, K. Yoshiuchi, Y. Yamasaki, I. Shimomura, T. Matsuoka, M. Mathsuia, *Endocr. J.* **2009**, *56*, 699–706.
- [32] E. C. Lee, E. Ha, S. Singh, L. Legesse, S. Ahmad, E. Karnaukhova, R. P. Donaldson, A. M. Jeremic, *Phys Chem Chem Phys.* **2013**, *15*, 12558–12571.
- [33] D. B. Zorov, M. Juhaszova, S. J. Sollott, *Biochim Biophys Acta* **2006**, *1757*, 509–517.
- [34] A. Masad, L. Hayes, B. J. Tabner, S. Turnbull, L. J. Cooper, N. J. Fullwood, M. J. German, F. Kametani, O. M. El-Agnaf, D. Allsop, *FEBS Lett.* **2007**, *581*, 3489–3493.
- [35] N. N. Louros, P. L. Tsiolaki, A. A. Zompra, E. V. Pappa, V. Magafa, G. Pairas, P. Cordopatis, C. Cheimonidou, I. P. Trougakos, V. A. Iconomidou, S. J. Hamodrakas, *Biopolymers* **2015**, *104*, 196–205.
- [36] T. Kowalik-Jankowska, A. Rajewska, K. Wiśniewska, Z. Grzonka, J. Jezer-ska, *J. Inorg. Biochem.* **2005**, *99*, 2282–2291.
- [37] P. Danyi, K. Várnagy, I. Sóvágó, I. Schön, D. Sanna, G. Micera, *J. Inorg. Biochem.* **1995**, *60*, 69–78.
- [38] A. Magri, A. Munzone, M. Peana, S. Medici, M. A. Zoroddu, O. Hansson, C. Satriano, E. Rizzarelli, D. La Mendola, *Int. J. Mol. Sci.* **2016**, *17*, 1240.
- [39] T. Kowalik-Jankowska, M. Ruta, K. Wiśniewska, L. Lankiewicz, *J. Inorg. Biochem.* **2003**, *95*, 270–282.
- [40] D. La Mendola, A. Magri, L. I. Vagliasindi, Ö. Hansson, R. P. Bonomo, E. Rizzarelli, *Dalton Trans.* **2010**, *39*, 10678–10684.

---

 Manuscript received: October 16, 2017

Accepted manuscript online: November 7, 2017

Version of record online: November 30, 2017